Chapter 5

Influences of Pathway Mutations on the Kinetics of CO Rebinding and NO Release in a Nitric Oxide Synthase

Reproduced with permission from Whited, C. A., Lavoie, K. D., Weinert, E. E., Agapie, T., Winkler, J. R., and Gray, H. B. Pathways of NO Release in Nitric Oxide Synthase. *submitted*. 2011.

5.1 Abstract

Nitric oxide synthases (NOS) are a family of enzymes responsible for the production of the signaling molecule nitric oxide (NO). The rate at which NO is released by each enzyme varies greatly among isoforms and species, over nearly two orders of magnitude. One residue (an isoleucine located above the heme in bacterial enzymes) involved in the gating of NO release has been previously identified by Stuehr. However, this single residue does not account for the entirety of the differences among the forms of NOS. Another residue, a histidine at position 134 in NOS from *Geobacillus stearothermophilus* (gsNOS), was hypothesized to also participate in gating NO release based on an observed correlation between rates of NO release and the bulk of side chains at this position. Each single point mutation, H134S and I223V, and the double mutant were expressed in gsNOS and their reactivity toward the diatomic molecules CO and NO were studied. CO rebinding was investigated using laser flash photolysis and NO release using stopped flow UV-visible spectroscopy. The presence of both monomer and dimer was observed in solution and position 134 was shown to be another key residue in gating NO release. Wild type gsNOS contains both the bulkier Ile223 and His134 and has the slowest measured NO release (0.039 s^{-1}) of all NOS enzymes. Each single mutation increased NO release substantially, while the double mutant has a rate constant of 1.0 s^{-1}, nearly as fast as mammalian iNOS at 2.3 s^{-1}, identifying position 134 as another important factor determining rate constants for NO release.

5.2 Introduction

Nitric oxide synthases (NOS) are found in all eukaryotes, as well as a selection of prokaryotes, and are responsible for biological production of nitric oxide (NO).[1-2] In mammals, various isoforms of NOS are involved in processes such as neurotransmission and vasodilation.[3] Interestingly, the immune system uses high levels of NO to kill invading bacterial cells. Given this function of NO, the discovery of NOS-like enzymes in bacteria was unexpected. The role of NO in these bacteria is still under debate, although it has been proposed to be a method to combat host immune responses.[4-6] Different functions most likely require different rates of NO release in cells. This can be controlled through several methods such as regulation of protein expression within a cell (as is the case for mammalian inducible NOS found in macrophages) or on the molecular level within the enzyme. These studies focus on the latter, namely the manner in which the enzyme itself regulates NO release.

Nitric oxide synthases contain a thiolate-ligated heme active site, very similar to that found in cytochromes P450.[7-8] This superfamily of enzymes carries out a vast array of biological oxidations, using the heme cofactor to activate dioxygen.[9] NOS, on the other hand, catalyzes only the oxidation of arginine to produce NO in two turnovers (through the enzyme-bound intermediate N-hydroxy-L-arginine). The first turnover involves a two-electron oxidation of substrate like cytochromes P450, while the second is formally a three-electron oxidation and is unique in biology.[10-11] What is known of the catalytic cycle is shown in **Scheme 5.1** colored black. The two species in blue are intermediates from the cycle of cytochromes P450 used to fill in gaps in our knowledge

of the NOS cycle. The numbers in red represent the pathways taken in each turnover and highlight the differences.

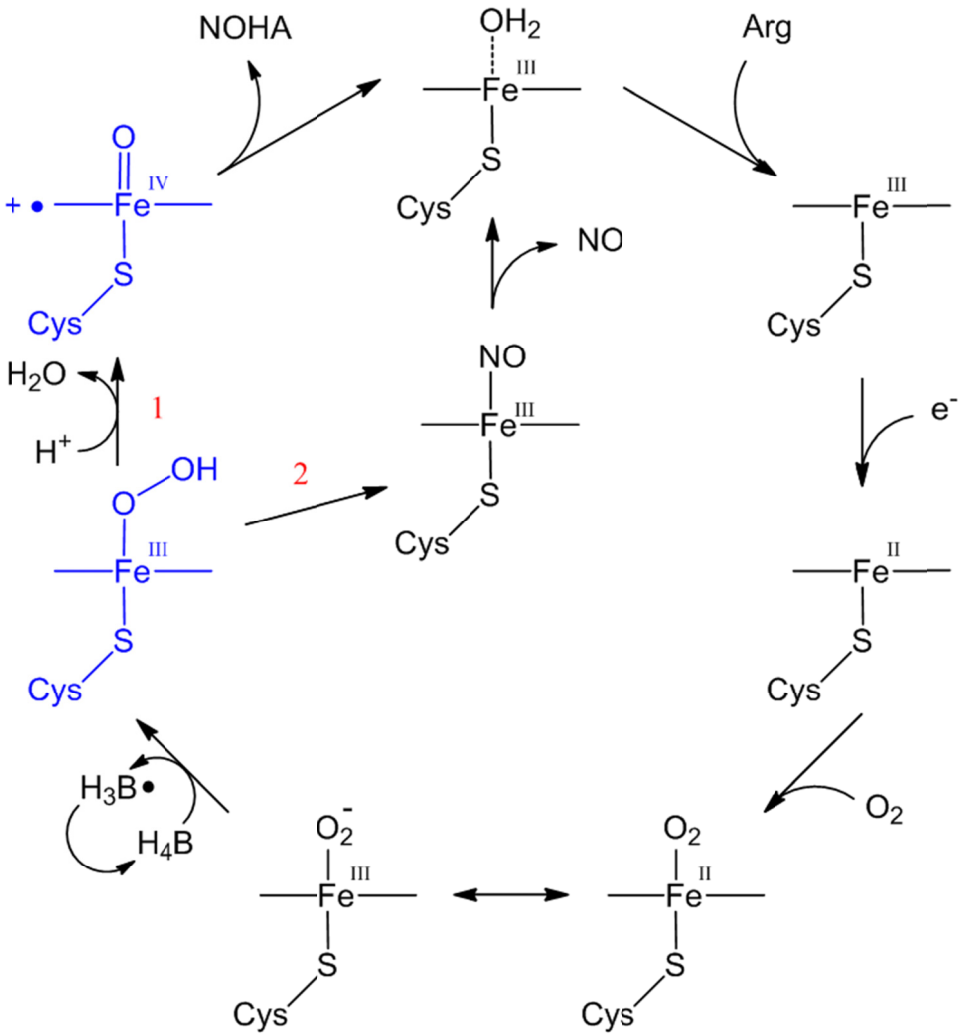

Scheme 5.1. A proposed catalytic cycle for both turnovers of NOS producing NO.

The last step of catalysis involves formation of a ferric-NO species which slowly releases the radical species NO. The ferrous-oxy and ferric-NO species are the only two intermediates observed during turnover and it is solely on the basis of the demonstrated cytochrome P450 cycle that the two compounds in blue are included. (There is some recent evidence for these from EPR and ENDOR studies, but they have not been

corroborated.[12]) However, multiple groups have demonstrated ferric-NO formation and its decay to release the radical species. In mammals, a series of complex steps has evolved in order to regulate enzyme function and keep tight control on each step, such as delivery of electrons and the tuning of redox potentials.[13] It is not fully understood how the protein matrix controls NO release and what factors cause this rate to vary among forms of NOS enzymes, nor how NO production is controlled in bacterial systems.

In order to study NO release, stopped flow UV-visible spectroscopy has been employed. The unique spectroscopic features of heme enzymes allow for the differentiation of various species during catalysis. Single turnover experiments, where the fully-reduced, substrate-bound enzyme is held in de-oxygenated buffer and then mixed rapidly with buffer that is saturated in oxygen, have allowed the determination of rates of NO release in many NOS enzymes.[14-17]

It was observed in such stopped flow measurements that while the mammalian NOS isoforms release NO on the order of 2 to 5 s^{-1}, many bacterial enzymes release NO about one order of magnitude slower.[16] Crystallographic studies reveal a valine residue in mammalian forms which is replaced with an isoleucine in many bacterial forms.[18-20] This isoleucine is within Van der Waals contact of any diatomic bound at the iron center. Stuehr and coworkers showed that installation of an isoleucine at this position in the mammalian inducible NOS slows the rate of NO release, while removal of this methyl group through mutation to a valine in the bacterial NOS from *Bacillus subtilus* increases its rate of NO release.[16] While this is an important finding, the rate constants do not change by the full order of magnitude that separates them (in iNOS, 2.3 s^{-1} slows to 0.77

and in bsNOS 0.23 increases to 0.82). Clearly additional factors modulate the rates of NO release.

Flash photolysis is another technique commonly used to study the interactions of diatomic molecules with proteins.[21-23] Most heme centers form stable complexes with carbon monoxide (CO) in the ferrous state.[7, 24] While indefinitely stable in the dark, when exposed to visible (green) light the iron-carbon bond of the ferrous-CO species is broken, liberating CO and transiently generating a five coordinate ferrous heme. Under an atmosphere of CO, the six-coordinate species is reformed.[25] Due to large differences between the absorbance spectra of the five- and six-coordinate heme species, transient absorption spectroscopy is again an ideal technique for observing reactivity.[25-26] CO is used preferentially over NO and O_2 because it alone is redox inactive. Exposure of reduced enzyme immediately leads to oxidation of the iron center. The lifetime of a ferrous-oxy species is incredibly short (milliseconds to seconds at best). Nature has been forced to take steps to prevent this reaction in order to prevent the release of superoxide into cells. If the protein is reduced when substrate and cofactor are not present, superoxide will certainly be released, leading to cellular damage. NO also undergoes redox chemistry with the ferrous iron to oxidize it. CO is the closest mimic that will not undergo the same chemical reactions. The interactions of CO with myoglobin,[27-30] microperoxidase-8,[31] human myeloperoxidase,[32] and cytochrome P450[33-35] have been previously studied extensively. It was found that CO is a good mimic for the study of oxygen binding to these biologically important proteins.[24, 29]

Both flash photolysis and stopped flow coupled with transient UV-visible spectroscopy were used to study the interactions of diatomics with the nitric oxide

synthase from *Geobacillus stearothermophilus* (gsNOS).[36-37] The wild type enzyme, with isoleucine in position 223 (gsNOS numbering) directly above the heme as is commonly found in bacterial enzymes, as well as three other mutant species were studied by both techniques. Site-directed mutagenesis was used to insert a valine at position 223, as previously demonstrated in bsNOS to increase the rate of NO release. Mutations were also made at position 134.

We have observed a correlation between reported rate constants of NO release in the literature with residues found at this position. We will call these two positions gates. bsNOS has a histidine residue at this alternate position and has a particularly small rate constant of 0.23 s^{-1}, while the NOS from *Deinococcus radiodurans*, also bacteria, has a larger release rate constant of 0.50 s^{-1} and a smaller alanine residue at this second gate.[38] Both bacterial enzymes have an isoleucine in the first gate, keeping the overall rate smaller than mammalian forms. The NOS from mammalian neurons,[39] however, has a larger release rate constant of 5 s^{-1} and both gating positions contain smaller residues, valine near the heme and a serine corresponding to position 134 in gsNOS. The enzyme with the fastest recorded release rate constant comes from the bacterium *Sorangium cellulosum*[17] which has a valine above the heme and glycine at the second gate, and releases NO at a rate of 7–10 s^{-1}. Clearly, smaller residues at these two positions correlate with faster release of NO, while bulkier groups at 134 and 223 slow down NO release.

A series of four variants of gsNOS were expressed: wild type, I223V, H134S, and the double mutant H134S/I223V. The wild type enzyme with the bulkier side chains was found to have the slowest reported NO release rate of 0.039 s^{-1} by stopped flow spectroscopy. Each single mutant increased this rate constant substantially, I223V to 0.30

s^{-1} and H134S to 0.16 s^{-1}. The double mutant increased the rate of NO release to 1.0 s^{-1}, nearly the same as the mammalian isoforms. These data show that position 134 is in fact another residue key to enzymatic regulation of NO release, along with the known valine/isoleucine mutation. These results, together with CO flash photolysis studies provide a clear picture of the interactions of both NO and CO with this biologically important enzyme.

5.3 Experimental Methods

Sample Preparation

The plasmid for the nitric oxide synthase from *Geobacillus stearothermophilus* was a gift from the lab of Brian Crane. This enzyme was expressed as previously described by Sudhamsu and Crane with no significant deviations in procedure.[36] The enzyme was overexpressed in *Escherichia coli* BL21 (DE3) cells. Cells were grown to an optical density of approximately 1.0–1.4 and induced by adding a solution containing iron(III) chloride, IPTG, and δ-aminolevulinic acid (Aldrich) to final concentrations of 125 mg/L, 100 μM, and 50 mg/L, respectively, in milliQ water. The pETDuet vector (Novagen) coded for a C-terminal cleavable His_6-tag so samples were purified using metal affinity chromatography. (This vector also confers chloramphenicol resistance to the cells, so 34 μg/mL of this antibiotic were added to all cultures in Luria broth.) The His_6-tag was then cleaved using bovine thrombin (Calbiochem). Both thrombin and the His-tag were removed using size exclusion chromatography. Sample purity and Soret band epsilon values were determined through use of the hemochromagen assay.

A QuikChange site-directed mutagenesis kit from Stratagene was used to make the desired mutations in the amino acid backbone. Primers were designed according to the guidelines outlined by the QuikChange kit manual. Unless otherwise noted, protein solutions were made in the following buffer: 50 mM Tris (2-amino-2-hydroxymethyl-propane-1,3-diol), 150 mM NaCl, pH 7.5 (the same buffer used for size exclusion chromatography). Steady-state UV-visible spectra were collected on an Agilent HP 8452 diode array spectrophotometer.

For laser experiments, oxygen-free samples were pumped into an anaerobic chamber (with an atmosphere of 100% N_2) and reduced under excess dithionite. A small excess of dithionite was left in samples in order to ensure that the heme center remained in the reduced, ferrous state throughout the entirety of the experiment. Samples were then placed in a quartz cuvette (Starna Cells) with a graded seal connecting the cuvette to a Köntes valve, enabling the secure sealing of the cuvette from atmosphere. The cuvettes were then sealed and removed from the anaerobic chamber. The side arm of the cuvette was attached to a Schlenk line and evacuated and backfilled with carbon monoxide (100% or 20% with 80% N_2) three times. Once the side arm was under the desired atmosphere of CO, the Köntes valve was opened to the side arm. The headspace of the cuvette, above the protein solution, was evacuated and back-filled with CO from the Schlenk line three times and sealed under this new atmosphere. The sample was gently shaken over night, in the dark, at 4 °C to allow for full equilibration of the atmosphere with the solution. Inadequate equilibration time resulted in irreproducibility between samples.

Formation of the ferrous-CO complex was confirmed using its characteristic absorption band at 446 nm. The stability of the sample was monitored by UV-visible spectroscopy after its generation, and immediately before and after laser irradiation. No samples showed significant degradation after irradiation by the laser.

Nanosecond Transient Absorption Spectroscopy

All transient UV-visible spectroscopic measurements for CO flash-photolysis experiments were conducted at the Beckman Institute Laser Resource Center at Caltech. For time-resolved measurements, a 10 Hz Q-switched Nd:YAG pulsed laser was used to provide 8 ns pulses of irradiation (Spectra-Physics Quanta-Ray PRO-Series). This laser was used to pump an optical parametric oscillator, which allows tuning pulses from the laser (355 nm output) in the visible region, between 400 and 650 nm (Spectra-Physics Quanta-Ray MOPO-700). The details of this setup have been previously described.[40] All samples were excited with 560 nm laser pulses and exposed to less than 5 mJ/pulse of power. All traces are an average of 500 laser shots using 1 nm slits.

Stopped Flow UV-Visible Spectroscopy

Samples were prepared anaerobically and transferred to an anaerobic tonometer with 1.5 equivalents of dithionite to scavenge any residual oxygen. Dithionite was used to scavenge oxygen from the stopped flow spectrophotometer (HiTech Scientific) syringes and excess dithionite was removed by repeated washing with anaerobic buffer. Protein samples (4–6 μM gsNOS, 60 μM H4B, and 200 μM N-hydroxy-L-arginine) were rapidly mixed with air saturated buffer at 4 °C. The formation and release of NO was monitored using a diode array detector and the rates fit globally using SpecFit32 (HiTech

Scientific). Measured rates were independent of protein concentration under these experimental conditions.

Data Analysis

Transient absorption traces were converted to optical density using Equation 5.1 and fit using Igor-Pro graphing software. All data were fit to a double exponential decay function, with residuals less than 1% of the signal.

5.4 Results

Steady-State Spectroscopy

UV-visible spectroscopy was used to characterize the resting state and to verify the formation of the ferrous-carbonyl species of each mutant sample. This technique is particularly useful given the sensitivity of heme absorption bands to their environment, ligation, and oxidation state. Each enzyme displayed a single Soret peak with an absorbance maximum at 446 nm as is typical for nitric oxide synthases and close to that of the related cytochromes P450, named for the sharp absorption of their ferrous-carbonyl species at 450 nm.[7] The spectra of several such forms of the wild type enzyme are shown in **Figure 5.1**.

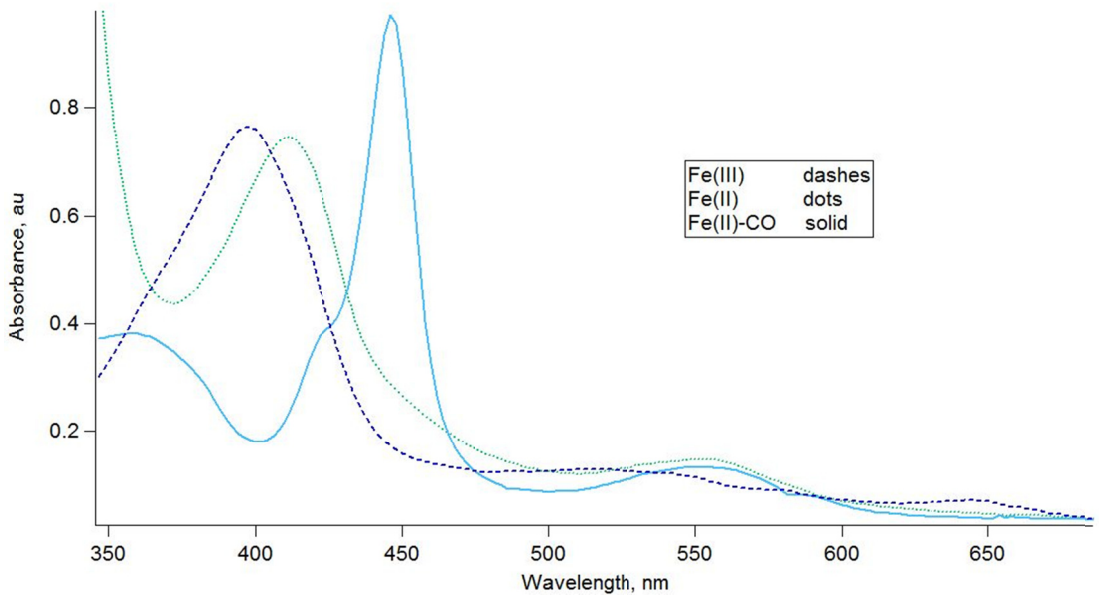

Figure 5.1. Absorption spectra of wild type gsNOS is three forms: ferric resting state (dashes), five-coordinate ferrous (dots), and the six-coordinate ferrous-CO complex (solid line). All samples are in the following buffer: 50 mM Tris, 150 mM NaCl, pH 7.5.

For flash photolysis experiments, 560 nm light was used to pump the sample, breaking the Fe-C bond of the ferrous-CO complex. This liberates CO and transiently generates a five-coordinate ferrous-heme complex. Both of these species can be generated and characterized under steady-state conditions (as shown above), allowing generation of the difference spectrum expected from transient studies. A trace of (Fe^{II})-(Fe^{II}-CO) difference spectrum for the wild type enzyme is shown in **Figure 5.2**.

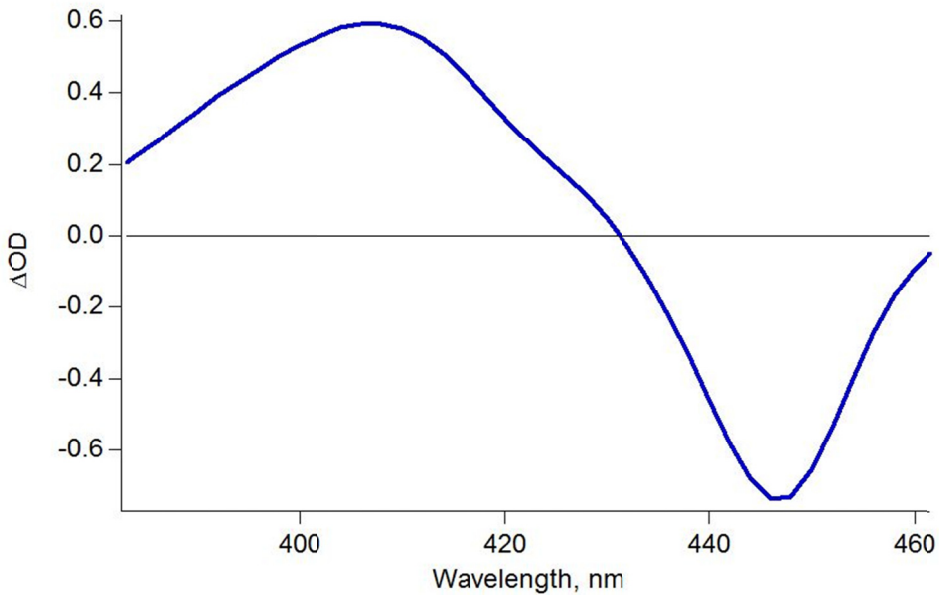

Figure 5.2. Steady-state difference spectrum produced by subtracting the spectrum of the wild type ferrous-CO complex from the five-coordinate ferrous species. This represents 100% conversion between species. Buffer: 50 mM Tris, 150 mM NaCl, pH 7.5.

CO Flash Photolysis

Upon irradiation with 560 nm light, CO is immediately liberated from the protein sample and the ferrous-CO complex reforms over the millisecond timescale. This rebinding process was monitored at 440 nm (near the maximum absorption of the six-coordinate species) and 410 nm (near the maximum absorption of the transiently-generated five-coordinate species). These two wavelengths give us separate handles on what should be the same kinetic process. Typical traces are shown in **Figure 5.3**. One can clearly see the signal bleach at 440 nm (B) upon loss of the CO complex and the signal from the transiently generated species at 410 nm (A), and that the two relax to ground state on roughly the same timescale.

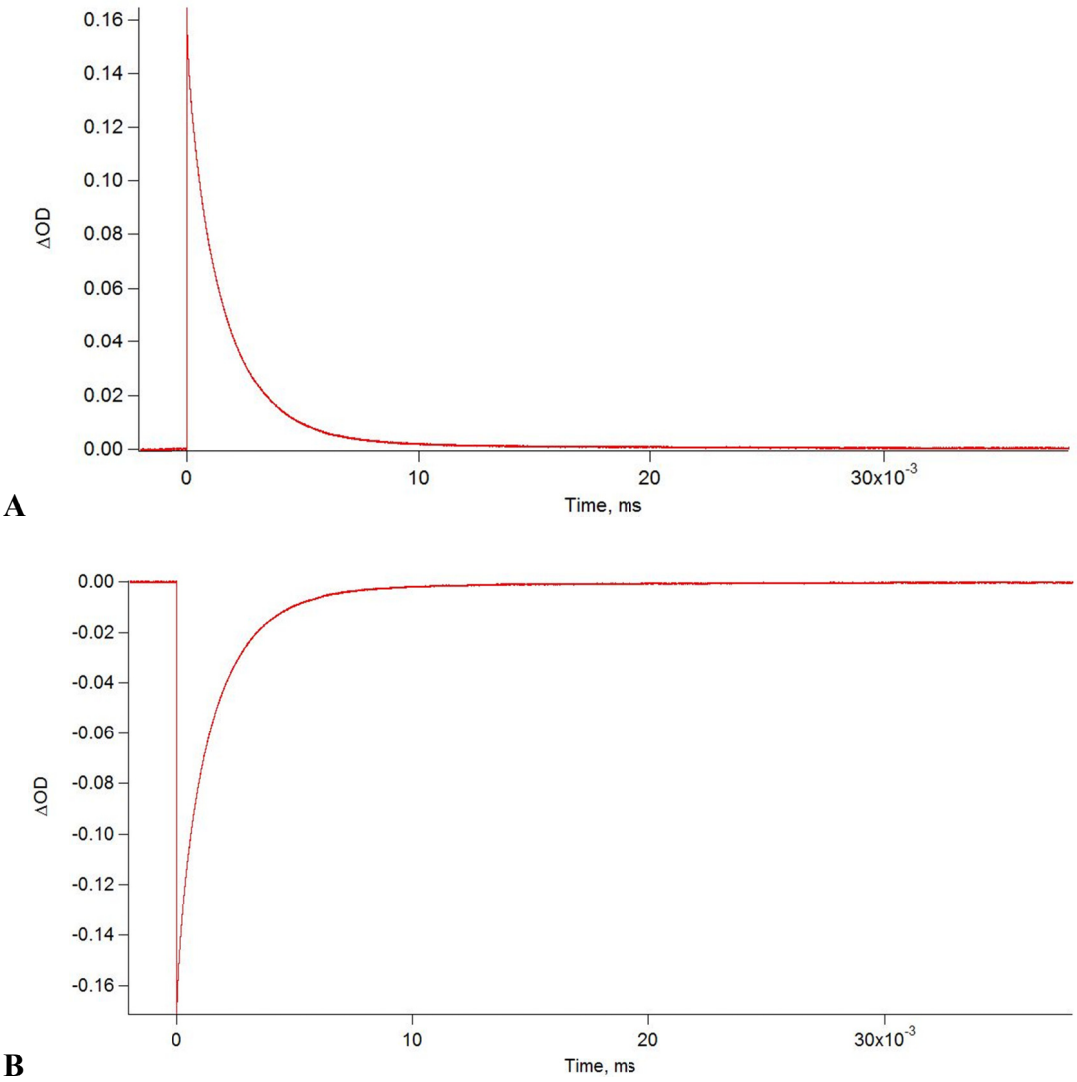

Figure 5.3. (A) Typical transient recorded at 410 nm, wild type enzyme, 40 ms timescale, 100% CO atmosphere. (B) Bleach upon loss of six-coordinate complex at 440 nm and its recovery. 6.1 μM enzyme, and buffer: 50 mM Tris, 150 mM NaCl, pH 7.5.

The current output generated at the detector (a nine-stage photon multiplier tube) was converted to change in optical density (OD) through the following equation,

$$\Delta OD = -\log(I/I_0) \qquad (5.1)$$

where I is the signal intensity and I_0 is the intensity before the laser pulse at t = 0. To confirm that the observed photochemical process is in fact dissociation of carbon monoxide and formation of the five-coordinate ferrous heme, a transient difference

spectrum was generated by collecting traces between 395 and 460 nm without alteration of the optics to maximize the signal. The signal at t = 1 ms was recorded for each wavelength (stepping every 5 nm), generating the following difference spectrum 1 ms after irradiation, **Figure 5.4** (note the similarity to the spectrum in **Figure 5.2**).

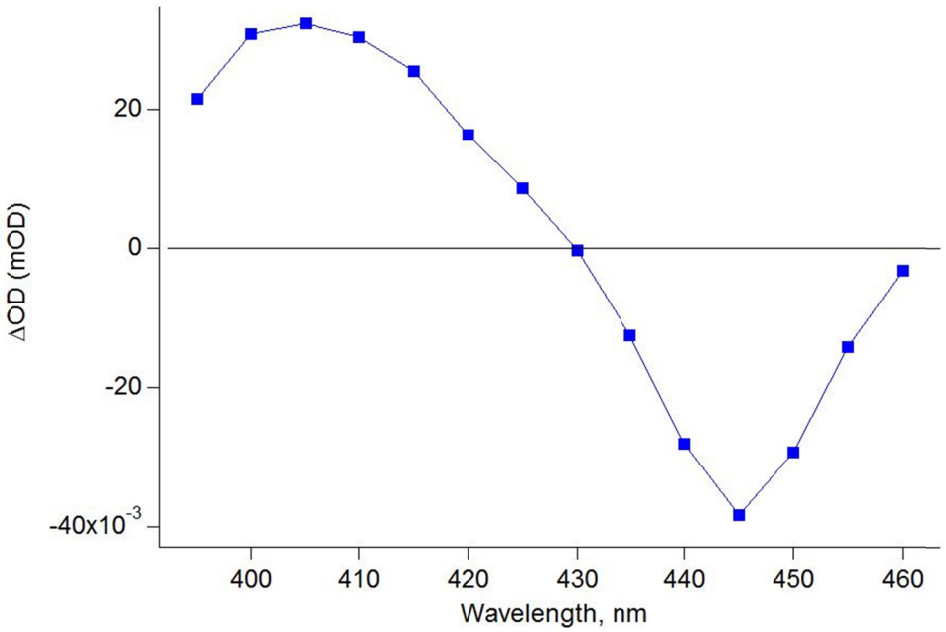

Figure 5.4. Transient difference spectrum generated 1 ms after laser pulse. 6.1 μM enzyme, and buffer: 50 mM Tris, 150 mM NaCl, pH 7.5.

Kinetics traces were collected at both 410 and 440 nm for each protein sample; all measurements were made at least in duplicate. Traces were fit using Igor Pro to a double exponential decay. This equation (5.2) provided the best fit to the data, yielding residuals of less than 1% of the signal strength. Kinetics parameters for each protein sample are given in **Table 5.1A**. Typical traces collected at 440 nm are shown in **Figure 5.5**.

$$y = A_1 \cdot \exp(-t/\tau_1) + A_2 \cdot \exp(-t/\tau_2) \qquad (5.2)$$

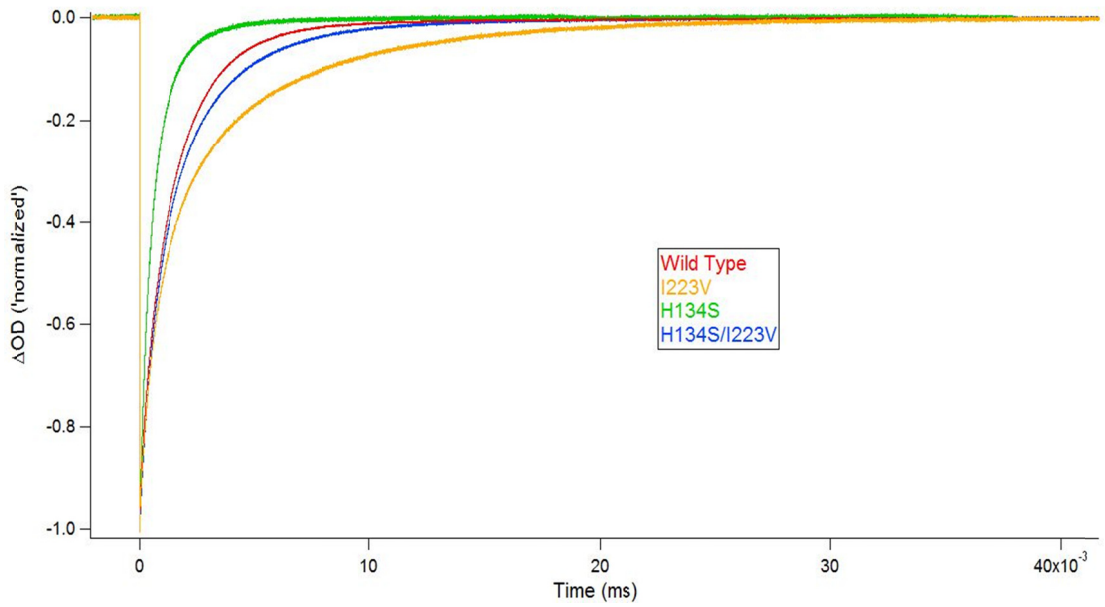

Figure 5.5. Typical kinetics traces for each of the four species studied (440 nm).

A double exponential decay was somewhat unexpected. In order to further characterize the kinetics, the dependence on CO concentration was analyzed. The concentration of CO in solution was altered by changing the content of CO in the gas filling the head space of each cuvette. The effects of CO concentration on the observed rate constants can be seen in **Table 5.1B**.

Table 5.1. CO recombination rates for both fast and slow second-order processes.

% CO, k_1 (s^{-1})	**WT**	**I223V**	**H134S**	**H134S/I223V**
(A)				
$100 - t_1$	510	190	750	310
$100 - t_2$	1500	1100	2400	1200
(B)				
$20 - t_1$	100	45	120	54
$20 - t_2$	390	240	370	240

We also analyzed the effect of these mutations on the pre-exponential factor of each rate from the double exponential fit. By introducing these small changes, we appear to be altering significantly the amount of the fast and slow phase, relative to one another. By introducing a single serine residue near the surface of the enzyme, the ratio of A1 to A2 is shifted from 2:1 to 1:2.

Table 5.2. Relative percentages of each rate constant by mutant.

100% CO	**WT**	**I223V**	**H134S**	**H134S/I223V**
A1 (t_1)	66%	46%	36%	43%
A2 (t_2)	34%	54%	64%	57%

Stopped-Flow UV-Visible Spectroscopy

NO release rates were measured for each protein sample using single turnover experiments. The enzyme was loaded with the redox active cofactor, tetrahydrobiopterin, and the substrate N-hydroxyarginine and then reduced using sodium dithionite. These samples were prepared anaerobically, sealed in a gas-tight syringe, and mixed with fully aerated buffer ($[O_2] \approx 258$ μM) to initiate turnover. Catalysis was monitored using UV-visible spectroscopy between 370 and 710 nm, with spectra taken at regular intervals over millisecond to second timescales. On faster timescales, the five-coordinate ferrous heme complex can be observed in the initial trace due to the excess dithionite present. Nearly immediately (within 5 ms, the dead time of the mixer), the ferrous-oxy species is formed; this formation is too rapid for stopped-flow spectroscopy to characterize the rate. (Note: dithionite reacts with oxygen several orders of magnitude faster than the enzymes under study and is therefore completely reacted before the second trace is collected.) The ferrous-oxy subsequently forms an intermediate complex, which finally decays to the resting ferric state of the enzyme (**Scheme 5.2**). In all cases, the first trace is discarded, as

the presence of a small amount of excess reductant (necessary to ensure the protein remains fully reduced) confuses the kinetics. All other traces are used in global fitting analysis using the SpecFit32 software package to extract spectra of all intermediates and rates of each species formation and/or decay. All spectral data were initially fit to a three-state kinetics model, with two rates to be extracted.[14, 16] This model was used in order to be consistent with all previously published analyses of NOS stopped-flow data. The traces of the first and last states, A and C, can be generated independently, A from mixing reduced enzyme with oxygenated buffer in the absence of substrate and cofactor. The ferrous-oxy species, A, decays over a period of approximately 90 s in the wild type enzyme at 4 °C, allowing for reliable characterization.[17] Species C is simply the resting, ferric, state of the enzyme. Thus, fitting software need only generate a single transient spectrum and two rates.

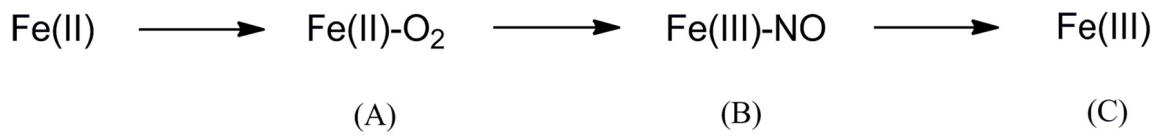

Scheme 5.2. Model for the conversion of the ferrous state of the enzyme to the resting ferric state (C), in the presence of oxygen, cofactor, and substrate through two intermediates: (A) a ferrous-oxy complex and (B) a ferric-NO complex.

From these experiments, several species can be characterized for each mutant enzyme, the ferrous-oxy and the putative ferric-NO, as well as the rate that the oxy complex reacts to form the NO complex and the rate that NO is subsequently released to form the resting five-coordinate ferric state. Typical traces collected are shown in **Figure 5.6** for the wild type enzyme. This work will focus only on the NO release rates, as formation rates of all samples were typical for NO synthases. Rate constants of NO release are listed in **Table 5.3**, along with the rates of NO release of other NOS enzymes.

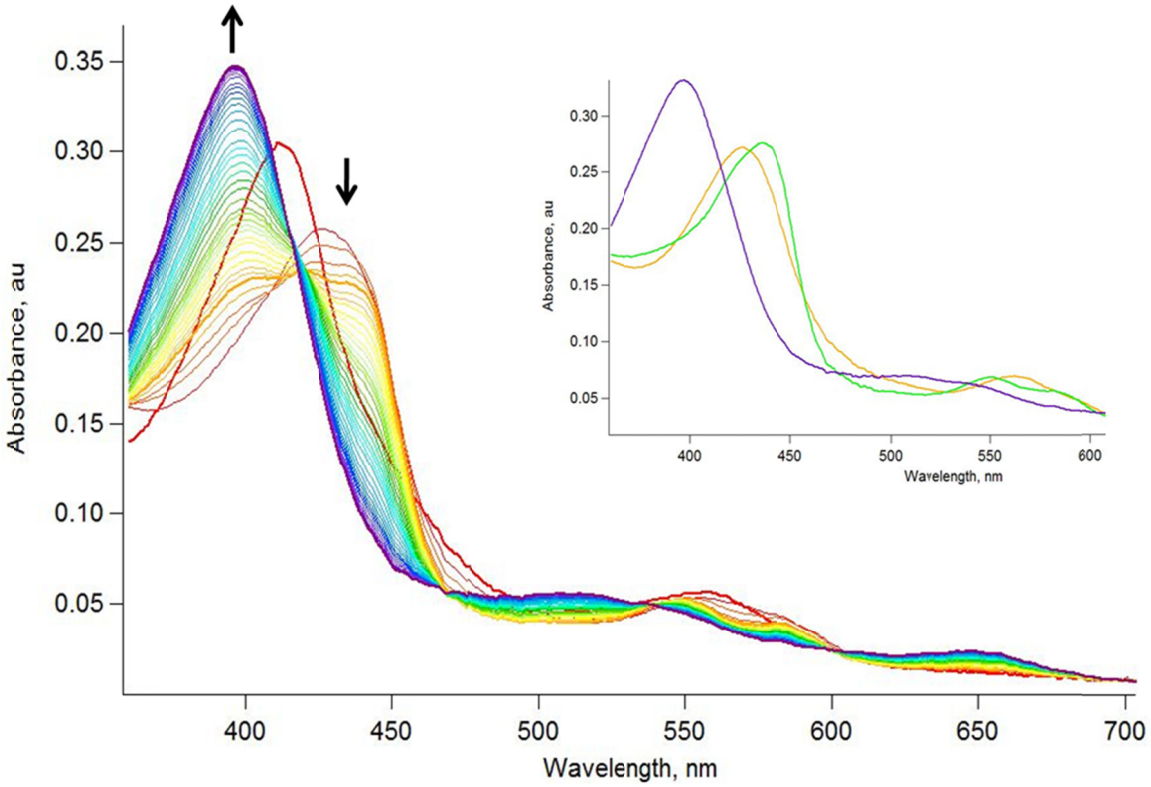

Figure 5.6. Transient spectra collected upon reaction of 4.5 µM reduced gsNOS (60 µM H4B and 200 µM N-hydroxy-L-arginine) with air-saturated buffer at 4 °C. Inset: spectra of intermediate species as generated by SpecFit32 using a three-state model.

Table 5.3. NO release rate constants of the four mutants in this study as well as three other NOS rates for comparison.[a]

Mutations	**Rate (s^{-1})**	**Gate 1**	**Gate 2**	**Temp. (°C)**	**Source**
wt	0.039	Ile	His	4	a
H134S	0.16	Ile	Ser	4	a
I223V	0.30	Val	His	4	a
H134S/I223V	1.0	Val	Ser	4	a
iNOS	2.3	Val	Ala	10	[16]
scNOS	7-10	Val	Gly	10	[17]
bsNOS	0.23	Ile	His	10	[16]

[a]iNOS has a rate typical for mammalian enzymes. bsNOS has a rate typical for bacterial enzymes. scNOS and gsNOS represent the fastest and slowest (respectively) release rates among NOS enzymes.

5.5 Discussion

CO Flash Photolysis

The kinetics of CO rebinding to proteins such as myoglobin has been studied extensively and two common themes stand out. First, second-order recombination occurs typically with a rate constant on the order of 10^5 to 10^6 M^{-1} s^{-1}, regardless of the size of the protein (wild type Mb: 6.5×10^5 and wild type $P450_{nor}$: 6.1×10^5).[28, 33] Second, for nearly all systems studied, a simple three-state kinetics model is consistent with all observed data (**Scheme 5.3**). With such a scheme, one would expect to observe two processes: fast, first-order geminate recombination (k_g) where CO never escapes the protein's binding pocket and a slower, second-order bimolecular recombination step (k_1) that is pseudo-first order under experimental conditions given the large excess of CO in solution. It has been previously noted that at room temperature under similar conditions (1 atm. of 100% CO in the sample headspace) no geminate process can be observed as essentially all of the CO has sufficient energy to leave the protein's interior and escape to solvent.[25, 41] In light of these results we initially expected the observed behavior to fit a single exponential decay, however in all samples such a model cannot provide a good fit for recorded traces; a double exponential decay must be invoked. (A comparison of the fits and residuals of both single and double exponential models is shown in **Figure 5.7**). Further, both processes occur on the millisecond timescale, ruling out the possibility of geminate recombination which occurs on much faster timescales.[42]

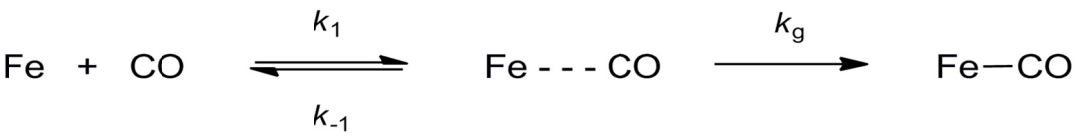

Scheme 5.3. Standard kinetics model for the recombination of CO with heme centers.[25, 27, 33] Fe represents the protein, k_g the geminate, and k_1 the second-order recombination.

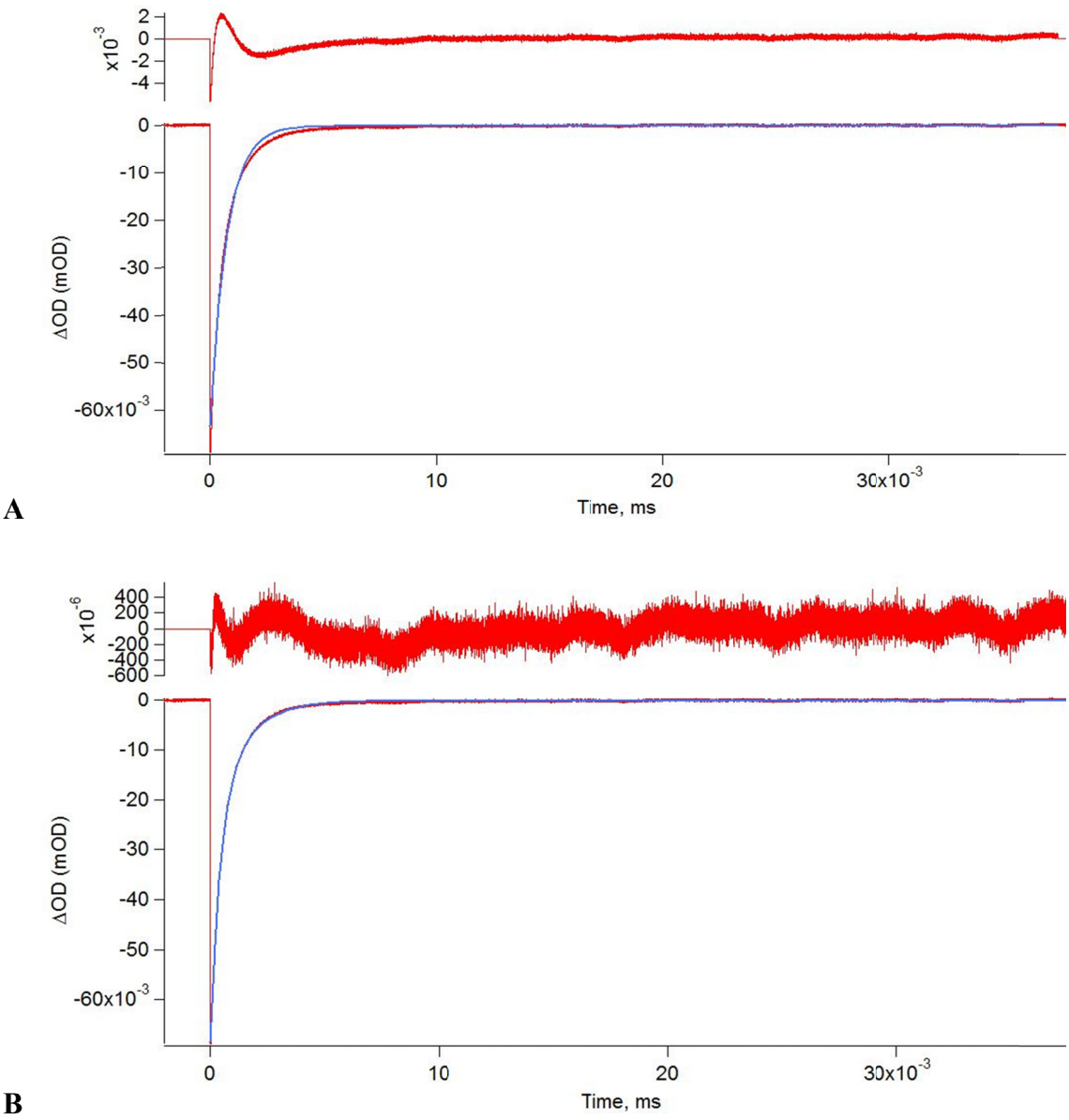

Figure 5.7. CO photolysis and rebinding under an atmosphere of 100% CO. Fits with residuals for both single exponential and double exponential decay models of transient data, typical of all four mutants. Fits are shown in blue above data (red). Residuals are shown in red on separate axes above the data. Note the scale of each y-axis.

To learn more about the two observed processes, we varied the percentage of CO in the headspace of samples. This reduction in CO concentration by one fifth lead to a decrease in CO rebinding rate constant for both processes in every sample, corresponding to about 1/4 to 1/6 of the previous rate. This indicates that both are first order in CO.

Further, the amplitudes of each exponential component of the fits are significant, with no one component accounting for less than 30% of the signal (**Table 5.2**). We hypothesized, given what is known about nitric oxide synthases and how they differ from other systems studied by this method, that we might be observing both the monomer and dimer in solution. It is known that NOS functions only as a dimer in mammals and disrupting dimerization shuts down catalysis.[1] During purification, bands for both monomer and dimer were observed on a size exclusion column in the same buffer with the same ionic strength. To test this hypothesis, samples were made with varying concentrations and we monitored the amplitude of both the faster and slower processes. **Table 5.4** shows the clear effect of concentration on the amplitudes of the faster and slower signals, consistent with the presence of monomer and dimer. Further, the two rate constants are similar in magnitude and both on the millisecond timescales, which agrees with both processes being second-order recombination with slightly different barriers. Introducing the presence of both monomer and dimer would account for the observed behavior of all samples.

Table 5.4. Effects of concentration on the relative proportion of the two processes. Concentration in μM.

[NOS]	A_1	A_2
6.1	64%	36%
9.9	58%	42%
27	35%	65%

Another possibility exists, however, as explanation for two observed millisecond processes. In proteins such as hemoglobin, a phenomenon called cooperativity is

observed.[43-44] When laser irradiation hits the sample, because of the large quantum yield for this photochemical process, a high percentage of photodissociation is observed. One can imagine a case where the protein exists completely as a dimer in solution and when irradiated either one or both bound CO molecules are librated. If cooperativity (or anti-cooperativity) is a contributing factor, dimers with a single CO molecule still bound would have a higher recombination rate constant than those where both are dissociated due to changes in protein conformation. In such a situation, the proportion of CO that is released from the protein will vary with laser intensity according to a standard power dependence and the proportion of the faster rate should decrease. A tenfold increase in laser power did not alter the proportion of the two rates observed, it merely increased the overall signal strength (**Table 5.5**).

Table 5.5. Power dependence of the relative amplitudes of each signal.

Power at sample (mJ/pulse)	$inv\tau_1$ (s^{-1})	$inv\tau_2$ (s^{-1})	A1	A2
0.6	91	9.9×10^2	58%	42%
0.7	91	1.0×10^3	57%	43%
2.8	88	9.6×10^2	59%	41%
6.4	87	9.4×10^2	59%	41%
7.0	87	9.4×10^2	59%	41%

From all these results we conclude that we are in fact observing both the monomer and dimer forms of the enzyme under experimental conditions, that both react with CO to give a rebinding rate constant on the order of 10^5 M^{-1} s^{-1} as has been found in other proteins, and propose the following kinetics model, **Scheme 5.4**.

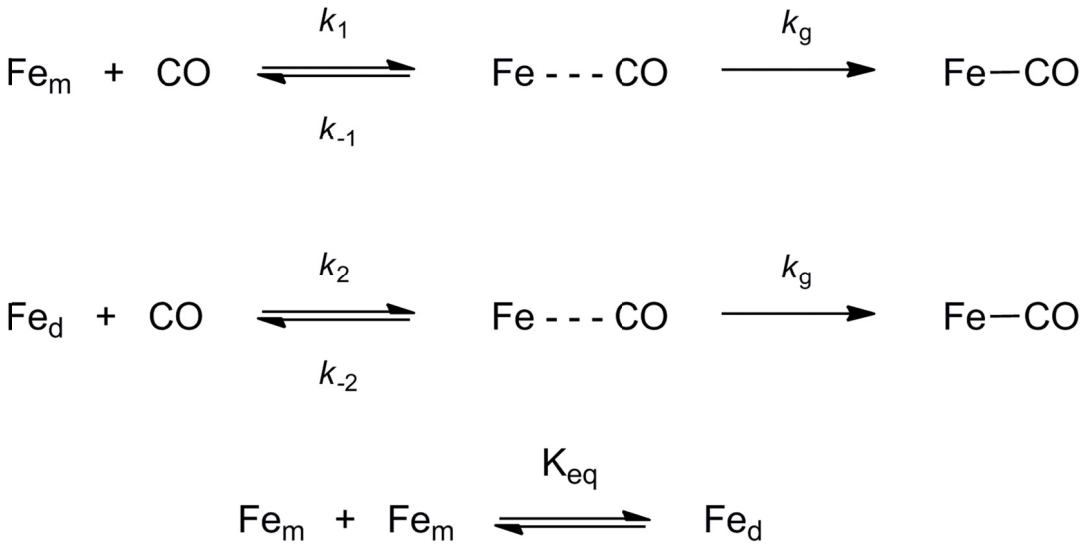

Scheme 5.4. A modified kinetics model for the recombintation of CO with gsNOS, incorporating the presence of both monomer and dimer forms of the enzyme. Fe represents the protein, k_g the geminate recombination rate, k_1 the second-order recombination rate for the monomer (Fe_m), and k_2 the second-order recombination rate for the dimer (Fe_d). Monomer and dimer must equilibrate on a slower timescale than CO recombination occurs.

From here, we can begin determining the effects of the point mutations that were made. The wild type enzyme has the two bulkiest groups at positions 134 and 223, histidine and isoleucine. These groups should slow the rate of diatomics traveling into and out of the protein's heme pocket. Thus, we hypothesized that the wild type would be the slowest of all the samples. The data show that while one mutant is faster than wild type (H134S), I223V is slower and the double mutant lies between the two single mutants, close to the wild type (**Figure 5.5**). The amplitudes of the fast and slow rate constants make it clear that each mutation affects not only the kinetics of second-order recombination events, but also the relative proportion of monomer and dimer in solution. This is consistent with our kinetics model in **Scheme 5.3**, however the competition between the two processes makes the two effects difficult to deconvolute.

NO Formation and Release

In order to determine the effect of these mutations on the NO release rate constant, we conducted single turnover experiments in the lab of Prof. Michael Marletta at UC Berkeley with the assistance of Dr. Emily Weinert. This allows for the direct comparison of our mutations with previously published rates of NO release. The wild type enzyme was found to release NO with a rate constant of 0.039 s^{-1}, which closely matches the rate constant previously published by Crane and Sudhamsu of 0.04 s^{-1}, under the same experimental conditions.[36] This enzyme has the smallest reported rate constant of all NOS enzymes. Each single mutation (H134S and I223V) increases the rate significantly, while the double mutant brings the rate to 1.0 s^{-1}, close to the higher rates found in mammalian enzymes (which were measured at a slightly higher temperature). The ability of a mutation at position 134 to both increase the rate on its own and to further increase the rate beyond the single mutation already known at position 223 (**Table 5.3**) confirms that it is in fact another key residue gating NO release.

Transient Spectra Generated by Modeling

During the fitting procedure, it was observed that the spectrum generated for the intermediate ferric-NO complex is not always consistent. For the fastest mutant, H134S/I223V, the ferric-NO species is nearly cleanly resolved, showing a peak near 440 nm (**Figure 5.8**). The slower mutants and the wild type enzyme showed a mixture of Soret bands (**Figure 5.9**). The observation of multiple bands like this clearly indicates that the model is incomplete — what is being fitted as a single intermediate is actually a mixture of species. This has been observed before in both a bacterial NOS and a slower mutant of a mammalian enzyme.[16] It has been proposed that the presence of the Ile near

the heme confines NO in the pocket.[19] A new model was developed in order to better fit the data and fully resolve these spectra.

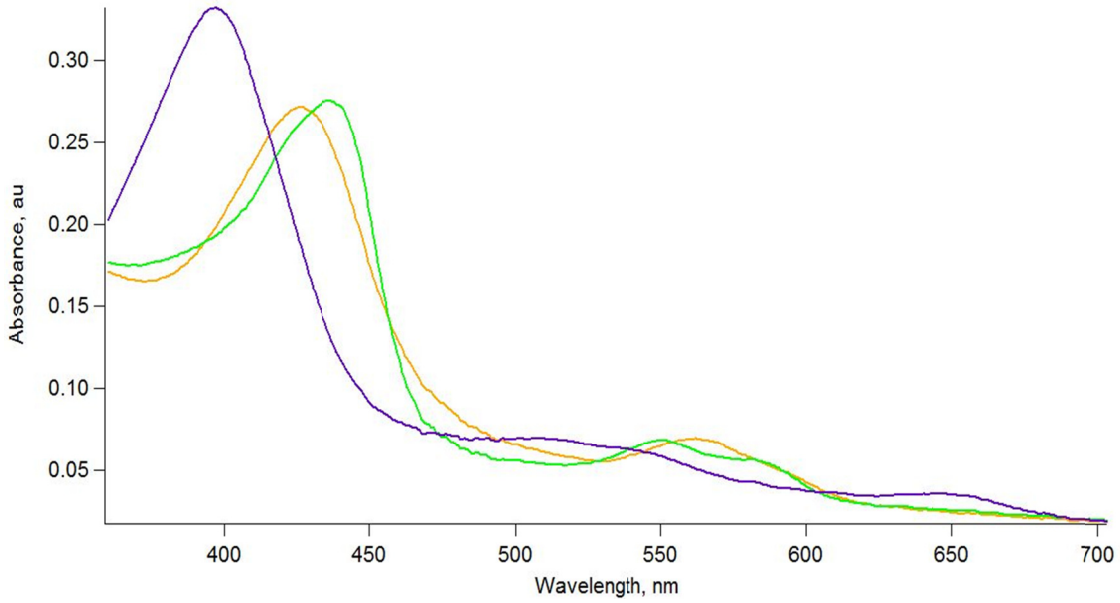

Figure 5.8 Spectra of intermediates generated by SpecFit software, for H134S/I223V gsNOS. Conditions: 50 mM Tris, 150 mM NaCl, pH 7.5, 4.4 µM NOS, 60 µM tetrahydrobiopterin, 200 µM N-hydroxy-L-arginine, approximately 130 µM oxygen. Green: ferric-NO, yellow: ferrous-oxy, purple: ferric resting state. Representative of single mutant I223V and the double mutant H134S/I223V.

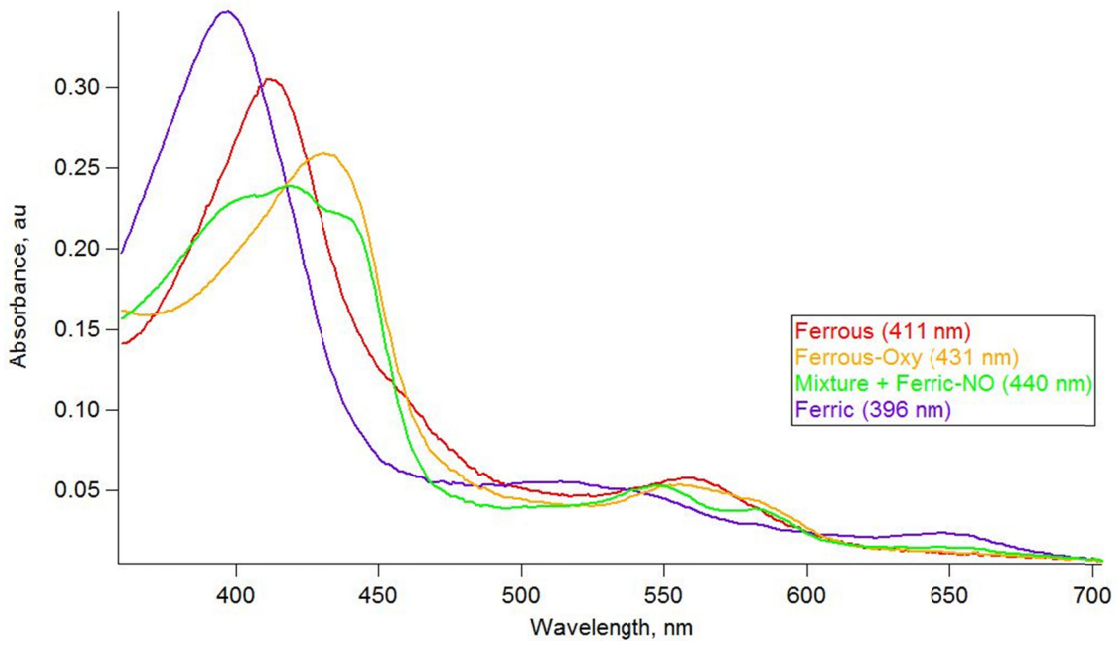

Figure 5.9. Spectra of intermediates generated by SpecFit software, for wild type gsNOS. Conditions: 50 mM Tris, 150 mM NaCl, pH 7.5, 4.4 µM NOS, 60 µM tetrahydrobiopterin, 200 µM N-hydroxy-L-arginine, approximately 130 µM oxygen. Yellow: ferric-oxy, green: ferric-NO, red: ferrous, purple: ferric resting state. Representative of both wild type and the single mutant H134S.

In order to fully resolve each individual species/intermediate, a five-state model was required. Any fewer species resulted in spectra with mixed Soret bands (as can be seen in green in **Figure 5.9**). It was also required that the three intermediate species be in rapid equilibrium with each other. This result fits well with the previously used three-state model. In the event that the equilibria favor the central species, the other two cannot be observed and the five-state model collapses to the three-state model. The final model used to fit all collected spectra is shown below (**Scheme 5.5**).

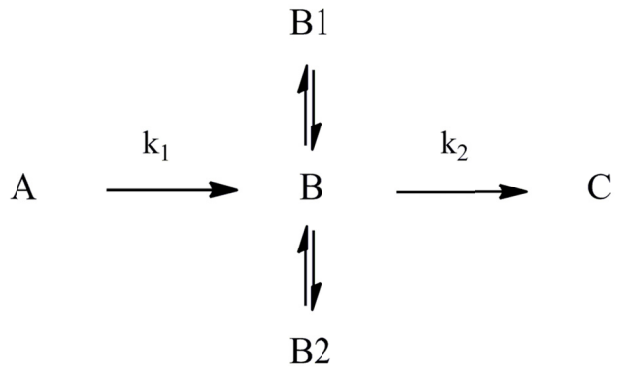

Scheme 5.5. The five-state model used to fit all transient stopped-flow data. B1 and B2 need not be off-pathway species, but all three B species must be in rapid equilibrium.

The above model fits all stopped-flow data well, resulting in reasonable rates and the generation of intermediate spectra with single Soret bands. Some extra information must be given to the fitting software, otherwise the system will be under-defined. When provided with the spectrum of B, in this case the ferric-NO species, and sufficiently large rates for each part of both equilibria, reasonable spectra and rates are calculated for A, B1, B2, C, k_1, and k_2. The values of k_2 for each enzyme as fitted by both models are shown in **Table 5.6**.

Table 5.6. Full kinetics details of fitting model for each of the four enzymes including a comparison of the NO release rate with the three-state model.

Enzyme	Process	Rate Constant	3-State Model's Fit
Wild Type	A > B	8.1×10^{-2}	
	B > B1	1.5×10^{5}	
	B1 > B	8.2×10^{4}	
	B > B2	1.5×10^{3}	
	B2 > B	2.9×10^{3}	
	B > C	**0.10**	**0.04**
H134S	A > B	1.7×10^{2}	
	B > B1	1.1×10^{6}	
	B1 > B	1.4×10^{6}	
	B > B2	1.6×10^{3}	
	B2 > B	6.7×10^{5}	
	B > C	**0.31**	**0.16**
I223V	A > B	1.0×10^{1}	
	B > B1	4.9×10^{4}	
	B1 > B	8.9×10^{4}	
	B > B2	1.2×10^{1}	
	B2 > B	1.6×10^{3}	
	B > C	**0.51**	**0.30**
H134S/I223V	A > B	1.6×10^{1}	
	B > B1	1.8×10^{4}	
	B1 > B	4.1×10^{0}	
	B > B2	1.4×10^{3}	
	B2 > B	1.9×10^{0}	
	B > C	**1.9**	**1.0**

In this model, A is the ferrous-oxy complex as before. Again, the spectrum of this species is well known and can be used to verify the accuracy and chemical reasonableness of the model and fit. The spectrum of B is specified as the ferric-NO spectrum with a maximum absorbance at 441 nm (courtesy of Dr. Joshua Woodward from the Marletta group), which is known to form during turnover. The spectrum of C is the final resting state of the enzyme, the five-coordinate ferric species. The spectrum

generated for one of the two new intermediates is essentially identical to that of the ferric resting state. This is consistent with an equilibrium between rapid release and rebinding of NO trapped in the binding pocket, which would be very fast when compared with the other processes occurring. It is also consistent that this would be seen to the greatest extent in the two enzymes with the Ile residue present near the heme. The methyl group of this residue is right at Van der Waals contact distance from any diatomoics bound to the iron and clearly blocks any exit from the binding pocket (as is clear from the crystal structure, PDB file 2FLQ).

The identity of the other intermediate is less obvious, but at least one reasonable possibility exists. The species is clearly formed after the majority of catalysis, being in equilibrium with the ferric-NO species. Several other models were applied, but the only one that fits the collected data is one where this species is in rapid equilibrium with the ferric-NO complex. As seen in **Figure 5.10**, this species has a Soret maximum near 420 nm. A species with a similar absorbance has been previously observed under catalytic conditions for the first turnover (Arg rather than NOHA was used as substrate).[15] This is also a slower enzyme, with a Trp to His mutation as discussed in Chapters 3 and 4, but made in the mammalian inducible NOS isoform. In this study, the authors proposed that this newly characterized species is Compound I.

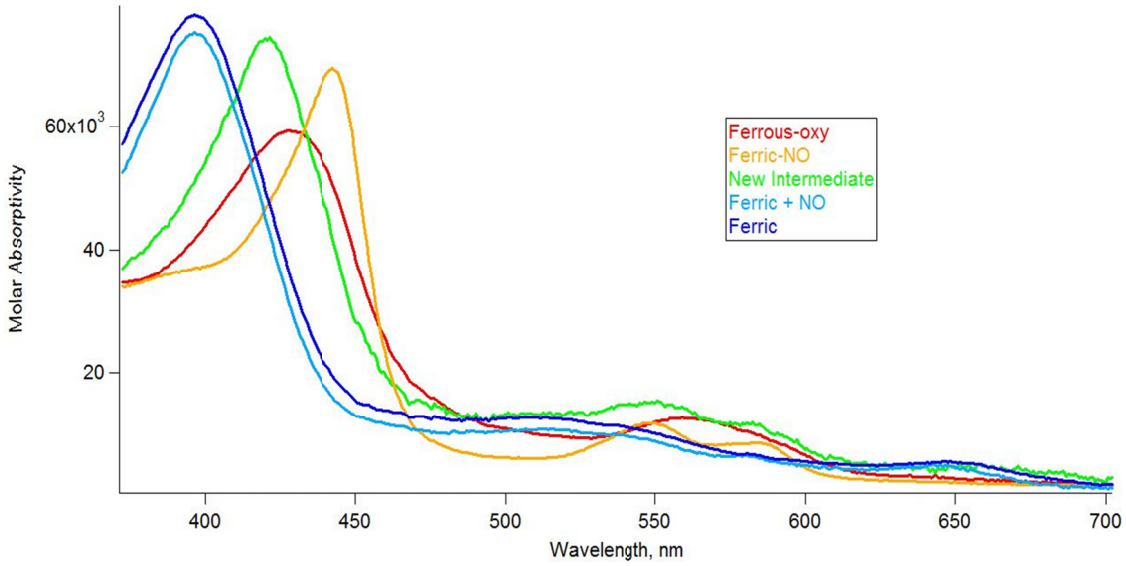

Figure 5.10. Spectra of all intermediate species in the five-state model of the wild type enzyme. All spectra match their reported literature values within ±2 nm, as well as the shape of the Q-bands. The identity of the species in green remains unknown.

Compound I is a Fe(IV)=O with another radical cation typically found on the porphyrin ring or another amino acid close to the heme center. This is formally a Fe(V) complex and is incredibly reactive. This complex was recently isolated and characterized and shown to react completely with substrate in less than 1 second, even in a thermophilic enzyme at 4 °C. In this NOS mutant, the complex with Soret band at 422 nm lives approximately 10–15 seconds at 10 °C before fully decaying. It is doubtful that such a reactive oxidant would live for that amount of time with substrate present and ready to be oxidized by the complex and Compound I has been shown to have a maximum absorption near 365 nm. We have made the same Trp to His mutation and saw no evidence for this species at 422 nm (see Chapter 4).

We propose that this species in our system may be either an HNO complex with the enzyme or a P420 form of the iron center. It is known that one electron from the heme complex must be sent back to the pterin cofactor to re-reduce it and release NO in the

second turnover.[45] The observed species may be the product heme complex before electron transfer to the pterin. The spectrum is nearly identical (simply 4 nm blue-shifted) of the spectrum of HNO-myoglobin.[46] However, this cannot be the species observed in the study of mammalian NOS, as they were probing the first turnover. An alternative explanation is that this 420 nm species is analogous to the P420 species (Chapter 3) where the thiolate ligand is protonated and/or dissociates. We may be observing the equilibrium between two protonation states of this ligand. Identification of a species based solely on a single UV-visible spectrum is difficult at best, but further attempts are being made to understand the origin of this spectrum.

5.6 Conclusions

First, CO is a valuable diatomic mimic for the more reactive dioxygen and nitric oxide, however with a caveat. One must remember the conditions under which experiments are performed. For CO photolysis, systems are under saturating conditions with large excesses of carbon monoxide. This is a good system for comparison with oxygen binding to hemoglobin in the lungs. Nitric oxide formation, on the contrary, involves the production of a single molecule of NO per protein, far from saturating conditions. Further, NO reacts rapidly in aerated aqueous solution, further preventing its buildup and keeping the system from reaching equilibrium. Also, the driving force ultimately behind each of these processes involves formation or cleavage of two distinct bonds. CO is very similar to NO, but on a fundamental level an Fe-N bond is not an Fe-C bond. While experiments with CO provide a wealth of information about the overall

kinetics model for reactivity with diatomics, for an NO release rate one must perform the single turnover experiments.

With these experiments, we have confirmed that the isoleucine residue at position 223 does gate NO release in gsNOS, slowing the decay of the ferric-NO species. We have also demonstrated that position 134, occupied by a histidine in wild type gsNOS, also gates NO release, with smaller residues at this position corresponding to faster release rates. Together, these two positions can account for the majority of the differences in rate between any two NOS enzymes.

Further, we have used a new, more accurate model to fit our data, showing rapid equilibrium between the bound and unbound NO, and another unidentified species. This species has been previously observed. It was called Compound I. The Compound I in cytochromes P450 has a much more blue-shifted Soret band with a maximum near 365 nm and it reacts much more quickly. It is of note that this species with absorbance at 420 nm has now been observed in both turnovers. Unfortunately, its identity remains a mystery.

5.7 References

1. Marletta, M. A. (1993) Nitric-oxide synthase structure and mechanism, *J. Biol. Chem. 268*, 12231.
2. Wei, C. C., Wang, Z. Q., and Stuehr, D. J. (2002) Nitric oxide synthase: Use of stopped-flow spectroscopy and rapid-quench methods in single-turnover conditions to examine formation and reactions of heme-o-2 intermediate in early catalysis, In *Enzyme kinetics and mechanism, pt f: Detection and characterization of enzyme reaction intermediates*, pp 320, Academic Press Inc, San Diego.
3. Alderton, W. K., Cooper, C. E., and Knowles, R. G. (2001) Nitric oxide synthases: Structure, function and inhibition, *Biochem. J. 357*, 593.
4. Gusarov, I., Shatalin, K., Starodubtseva, M., and Nudler, E. (2009) Endogenous nitric oxide protects bacteria against a wide spectrum of antibiotics, *Science 325*, 1380.
5. Gusarov, I., Starodubtseva, M., Wang, Z. Q., McQuade, L., Lippard, S. J., Stuehr, D. J., and Nudler, E. (2008) Bacterial nitric-oxide synthases operate without a dedicated redox partner, *J. Biol. Chem. 283*, 13140.
6. Johnson, E. G., Sparks, J. P., Dzikovski, B., Crane, B. R., Gibson, D. M., and Loria, R. (2008) Plant-pathogenic streptomyces species produce nitric oxide synthase-derived nitric oxide in response to host signals, *Chem. Biol. 15*, 43.
7. Dawson, J. H., and Sono, M. (1987) Cytochrome.P-450 and chloroperoxidase - thiolate-ligated heme enzymes - spectroscopic determination of their active-site structures and mechanistic implications of thiolate ligation, *Chem. Rev. 87*, 1255.
8. Gorren, A. C. F., and Mayer, B. (2007) Nitric-oxide synthase: A cytochrome p450 family foster child, *Biochimica Et Biophysica Acta-General Subjects 1770*, 432.
9. Sono, M., Roach, M. P., Coulter, E. D., and Dawson, J. H. (1996) Heme-containing oxygenases, *Chem. Rev. 96*, 2841.
10. Stuehr, D., Pou, S., and Rosen, G. M. (2001) Oxygen reduction by nitric-oxide synthases, *J. Biol. Chem. 276*, 14533.
11. Stuehr, D. J., Santolini, J., Wang, Z. Q., Wei, C. C., and Adak, S. (2004) Update on mechanism and catalytic regulation in the no synthases, *J. Biol. Chem. 279*, 36167.
12. Davydov, R., Sudhamsu, J., Lees, N. S., Crane, B. R., and Hoffman, B. M. (2009) Epr and endor characterization of the reactive intermediates in the generation of no by cryoreduced oxy-nitric oxide synthase from geobacillus stearothermophilus, *J. Am. Chem. Soc. 131*, 14493.
13. Stuehr, D. J., Tejero, J., and Haque, M. M. (2009) Structural and mechanistic aspects of flavoproteins: Electron transfer through the nitric oxide synthase flavoprotein domain, *Febs Journal 276*, 3959.
14. Boggs, S., Huang, L. X., and Stuehr, D. J. (2000) Formation and reactions of the heme-dioxygen intermediate in the first and second steps of nitric oxide synthesis as studied by stopped-flow spectroscopy under single-turnover conditions, *Biochemistry 39*, 2332.
15. Tejero, J. S., Biswas, A., Wang, Z. Q., Page, R. C., Haque, M. M., Hemann, C., Zweier, J. L., Misra, S., and Stuehr, D. J. (2008) Stabilization and characterization

of a heme-oxy reaction intermediate in inducible nitric-oxide synthase, *J. Biol. Chem. 283*, 33498.

16. Wang, Z. Q., Wei, C. C., Sharma, M., Pant, K., Crane, B. R., and Stuehr, D. J. (2004) A conserved val to ile switch near the heme pocket of animal and bacterial nitric-oxide synthases helps determine their distinct catalytic profiles, *J. Biol. Chem. 279*, 19018.
17. Agapie, T., Suseno, S., Woodward, J. J., Stoll, S., Britt, R. D., and Marletta, M. A. (2009) No formation by a catalytically self-sufficient bacterial nitric oxide synthase from sorangium cellulosum, *Proc. Natl. Acad. Sci. U. S. A. 106*, 16221.
18. Sudhamsu, J., and Crane, B. R. (2009) Bacterial nitric oxide synthases: What are they good for?, *Trends Microbiol. 17*, 212.
19. Beaumont, E., Lambry, J. C., Wang, Z. Q., Stuehr, D. J., Martin, J. L., and Slama-Schwok, A. (2007) Distal va1346ile mutation in inducible no synthase promotes substrate-dependent no confinement, *Biochemistry 46*, 13533.
20. Salard, I., Mercey, E., Rekka, E., Boucher, J. L., Nioche, P., Mikula, I., Martasek, P., Raman, C. S., and Mansuy, D. (2006) Analogies and surprising differences between recombinant nitric oxide synthase-like proteins from staphylococcus aureus and bacillus anthracis in their interactions with l-arginine analogs and iron ligands, *J. Inorg. Biochem. 100*, 2024.
21. Gautier, C., Mikula, I., Nioche, P., Martasek, P., Raman, C. S., and Slama-Schwok, A. (2006) Dynamics of no rebinding to the heme domain of no synthase-like proteins from bacterial pathogens, *Nitric Oxide-Biol. Chem. 15*, 312.
22. Feng, C. J., Thomas, C., Holliday, M. A., Tollin, G., Salerno, J. C., Ghosh, D. K., and Enemark, J. H. (2006) Direct measurement by laser flash photolysis of intramolecular electron transfer in a two-domain construct of murine inducible nitric oxide synthase, *J. Am. Chem. Soc. 128*, 3808.
23. Scheele, J. S., Bruner, E., Kharitonov, V. G., Martasek, P., Roman, L. J., Masters, B. S. S., Sharma, V. S., and Magde, D. (1999) Kinetics of no ligation with nitric-oxide synthase by flash photolysis and stopped-flow spectrophotometry, *J. Biol. Chem. 274*, 13105.
24. Phillips, G. N., Teodoro, M. L., Li, T. S., Smith, B., and Olson, J. S. (1999) Bound co is a molecular probe of electrostatic potential in the distal pocket of myoglobin, *J. Phys. Chem. B 103*, 8817.
25. Austin, R. H., Beeson, K. W., Eisenstein, L., Frauenfelder, H., and Gunsalus, I. C. (1975) Dynamics of ligand-binding to myoglobin, *Biochemistry 14*, 5355.
26. Springer, B. A., Sligar, S. G., Olson, J. S., and Phillips, G. N. (1994) Mechanisms of ligand recognition in myoglobin, *Chem. Rev. 94*, 699.
27. Cao, W. X., Ye, X., Georgiev, G. Y., Berezhna, S., Sjodin, T., Demidov, A. A., Wang, W., Sage, J. T., and Champion, P. M. (2004) Proximal and distal influences on ligand binding kinetics in microperoxidase and heme model compounds, *Biochemistry 43*, 7017.
28. Cao, W. X., Ye, X., Sjodin, T., Christian, J. F., Demidov, A. A., Berezhna, S., Wang, W., Barrick, D., Sage, J. T., and Champion, P. M. (2004) Investigations of photolysis and rebinding kinetics in myoglobin using proximal ligand replacements, *Biochemistry 43*, 11109.

29. Olson, J. S., Soman, J., and Phillips, G. N. (2007) Ligand pathways in myoglobin: A review of trp cavity mutations, *IUBMB Life 59*, 552.
30. Kleinert, T., Doster, W., Leyser, H., Petry, W., Schwarz, V., and Settles, M. (1998) Solvent composition and viscosity effects on the kinetics of co binding to horse myoglobin, *Biochemistry 37*, 717.
31. Park, J., Lee, T., and Lim, M. (2010) Viscosity-dependent dynamics of co rebinding to microperoxidase-8 in glycerol/water solution, *J. Phys. Chem. B 114*, 10897.
32. Murphy, E. J., Marechal, A., Segal, A. W., and Rich, P. R. (2010) Co binding and ligand discrimination in human myeloperoxidase, *Biochemistry 49*, 2150.
33. Shiro, Y., Kato, M., Iizuka, T., Nakahara, K., and Shoun, H. (1994) Kinetics and thermodynamics of co binding to cytochrome p450(nor), *Biochemistry 33*, 8673.
34. Ionascu, D., Gruia, F., Ye, X., Yu, A. C., Rosca, F., Beck, C., Demidov, A., Olson, J. S., and Champion, P. M. (2005) Temperature-dependent studies of no recombination to heme and heme proteins, *J. Am. Chem. Soc. 127*, 16921.
35. Campbell, B. N., Araiso, T., Reinisch, L., Yue, K. T., and Hager, L. P. (1982) A kinetic-study of the binding of carbon-monoxide to ferrous chloroperoxidase, *Biochemistry 21*, 4343.
36. Sudhamsu, J., and Crane, B. R. (2006) Structure and reactivity of a thermostable prokaryotic nitric-oxide synthase that forms a long-lived oxy-heme complex, *J. Biol. Chem. 281*, 9623.
37. Kabir, M., Sudhamsu, J., Crane, B. R., Yeh, S. R., and Rousseau, D. L. (2008) Substrate-ligand interactions in geobacillus stearothermophilus nitric oxide synthase, *Biochemistry 47*, 12389.
38. Reece, S. Y., Woodward, J. J., and Marletta, M. A. (2009) Synthesis of nitric oxide by the nos-like protein from deinococcus radiodurans: A direct role for tetrahydrofolate, *Biochemistry 48*, 5483.
39. Zhou, L., and Zhu, D. Y. (2009) Neuronal nitric oxide synthase: Structure, subcellular localization, regulation, and clinical implications, *Nitric Oxide-Biol. Chem. 20*, 223.
40. Dempsey, J. L., Winkler, J. R., and Gray, H. B. (2010) Kinetics of electron transfer reactions of h-2-evolving cobalt diglyoxime catalysts, *J. Am. Chem. Soc. 132*, 1060.
41. Doster, W., Beece, D., Bowne, S. F., Diiorio, E. E., Eisenstein, L., Frauenfelder, H., Reinisch, L., Shyamsunder, E., Winterhalter, K. H., and Yue, K. T. (1982) Control and ph-dependence of ligand-binding to heme-proteins, *Biochemistry 21*, 4831.
42. Gibson, Q. H., Regan, R., Elber, R., Olson, J. S., and Carver, T. E. (1992) Distal pocket residues affect picosecond ligand recombination in myoglobin - an experimental and molecular-dynamics study of position 29 mutants, *J. Biol. Chem. 267*, 22022.
43. Perrella, M. (1999) Understanding mechanisms in a cooperative protein: The co ligation intermediates of hemoglobin, *Biophys. Chem. 81*, 157.
44. Bellelli, A. (2010) Hemoglobin and cooperativity: Experiments and theories, *Curr. Protein Pept. Sc. 11*, 2.

45. Gorren, A. C. F., Sorlie, M., Andersson, K. K., Marchal, S., Lange, R., and Mayer, B. (2005) Tetrahydrobiopterin as combined electron/proton donor in nitric oxide biosynthesis: Cryogenic uv-vis and epr detection of reaction intermediates, In *Nitric oxide, pt e*, pp 456.
46. Farmer, P. J., and Sulc, F. (2005) Coordination chemistry of the hno ligand with hemes and synthetic coordination complexes, *J. Inorg. Biochem. 99*, 166.